NICOLAUS COPERNICUS UNIVERSITY IN TORUŃ

Bulletin of Geography. Physical Geography Series, No. 27 (2024): 87–109
http://doi.org/10.12775/bgeo-2024-0012

Comparative assessment of a flash flood susceptibility map based on morphometric analysis and bivariate statistics in the Upper Citarum Watershed, Indonesia

Fitriany Amalia Wardhani*[1,a], Elenora Gita Alamanda Sapan[1,b], Nicko Widiatmoko[1,c], Muhammad Ravi Yuvhenmindo[2,d], Budi Heru Santosa[1,e], Wiwiek Dwi Susanti[1], Andrea Emma Pravitasari[3,4], Endra Triwisesa[1], Iwan Ridwansyah[1]

[1]Research Center for Limnology and Water Resources, National Research and Innovation Agency (BRIN), Jl. Raya Jakarta-Bogor, Cibinong, Bogor, Indonesia
[2]Master's Program in Civil Engineering, Faculty of Civil and Environmental Engineering, Bandung Institute of Technology (ITB), Bandung, Indonesia
[3]Division of Regional Development Planning, Department of Soil Science and Land Resouces, Faculty of Agriculture, IPB University, Jl. Meranti, IPB Dramaga Campus, Dramaga, Bogor, Indonesia
[4]Center for Regional, Systems, Analysis, Planning, and Development (CRESTPENT/P4W), IPB University, Jl. Raya Pajajaran, Bogor, Indonesia

*E-mail: fitr024@brin.go.id

[a]https://orcid.org/0009-0008-1297-3068 ,[b]https://orcid.org/0000-0003-0621-8070 ,[c]https://orcid.org/0009-0009-6938-6785, [d]https://orcid.org/0009-0007-3396-8631 ,[e]https://orcid.org/0000-0001-5432-6821

Abstract. Flash floods are one of the most destructive natural disasters, characterized by rapid occurrence and high casualty rates due to a lack of preparedness. Mapping susceptibility areas to identify flash-flood-prone zones can be an effective tool for mitigation. Despite various flood susceptibility mapping methodologies, research on the most suitable statistical approach for Indonesia's unique environmental context remains limited. This study aimed to compare the performance of three statistical methods, namely Shannon's Entropy (SE), Statistical Index (SI) and Frequency Ratio (FR), in assessing flash flood susceptibility. Conducted in the Upper Citarum Watershed, Indonesia, this study used geospatial analysis using elevation, slope, curve number, lithology, soil movement, rainfall and morphometric parameters of the watershed to analyze flash flood susceptibility in the study area, with morphometric characteristics affecting hydrological processes such as surface runoff and soil erosion. The results indicate that the Statistical Index Flash Flood Susceptibility Map (SI FFSM) is the most effective model for representing flash flood susceptibility, achieving the highest AUC values for success rate (0.907) and prediction rate (0.933). According to the SI method, the three most influential parameters driving flash floods in the research area are elevation, landslides or soil movement, and rainfall. The total high and very high flash flood susceptibility area is 102.29 km2 or 46.95% of the study area. The findings of this study will contribute to the development of more-accurate and -practical tools for disaster risk assessment and management, both in Indonesia and other regions with similar environmental conditions.

Key words:
bivariate statistics,
flash flood susceptibility,
morphometric analysis,
statistical index,
susceptibility map,
Indonesia

Introduction

Floods are the most common type of natural disaster worldwide, causing many casualties and property losses (UNISDR 2015). The frequency and intensity of floods continue to increase due to human activities, such as rapid population growth and urban development, which directly increase the risk of flooding (Jain et al. 2022). Among the various types of floods, flash floods are the most

destructive because they occur suddenly, at high speed, and in a short time. This condition worsens when flash floods occur at night when people are resting, causing significant loss of life and property, especially to vulnerable groups (Rahman et al. 2016; Diakakis et al. 2020). Flash floods are generally triggered by extreme rainfall or rain falling on saturated soil, which has recently become more frequent due to climate change (Sayama et al. 2020; Cea and Costabile 2022). Practical mitigation efforts are needed to overcome this with a comprehensive understanding of flood's driving factors and dynamics, including rainfall-runoff processes, flood hydraulics, and discharge estimation (Jehanzaib et al. 2022). One important implementation is preparing a flash flood susceptibility map containing information on areas of various susceptibility classes, which can be used as a basis for early warning systems and disaster preparedness and response strategy planning (Mahmood and Rahman 2019).

Many studies have assessed the level of flash flood susceptibility of an area using morphometric parameters or prioritized sub-watersheds in flash flood mitigation strategies (Obeidat et al. 2021; Dutal 2023). In addition, various other physical parameters, such as elevation, slope, soil type, vegetation and others, can be used to analyze the potential for flash flood hazards. The Flash Flood Potential Index (FFPI) is one method used to estimate the potential for flash-flood-prone areas based on several parameters. This method was first applied in the Colorado Watershed, United States, using slope, vegetation, soil type and land use parameters (Costache and Zaharia 2017). Furthermore, FFPI has been modified by integrating other methods, including statistical approaches (Costache and Tien Bui 2019; Aleksova et al. 2024; Mansour et al. 2024).

In the development of flood hazard assessment, many researchers have proposed various models. Most of these models focus on hydrological models, hydrodynamic models, multicriterion decision analysis (MCDA), and bivariate statistical models such as Frequency Ratio (FR), Shannon's Entropy (SE), Statistical Index (SI), Weight of Evidence (WoE), and Machine Learning (ML) techniques integrated with Geographic Information Systems (GIS) (Khosravi et al. 2016; Costache and Tien Bui 2019; Mansour et al. 2024). The FR method is one of a popular method used for flood and flash flood research (Khosravi et al. 2016; Rahmati et al. 2016; Costache and Zaharia 2017; Samanta et al. 2018; Costache and Tien Bui 2019; Sarkar and Mondal 2020). In addition, several flash flood analyses have been conducted using SE analysis (Arora et al. 2021; Islam et al. 2022) and SI analyses (Cao et al. 2016; Tehrany et al. 2019). Comparison between SE, SI and Weighting Factor (WF) methods in previous studies (Khosravi et al. 2016; Samanta et al. 2018) on flash flood disasters showed that the SI method produced the best results, with the highest prediction and success rates (Khosravi et al. 2016). Meanwhile, when comparing the FR and SE methods for flood disasters, the FR method showed better validation performance than the SE method (Arora et al. 2021). However, there is still a gap in understanding the comparative efficacy of these methods in various real-world conditions, especially in tropical regions with complex topography and diverse geological characteristics.

Indonesia, located in the tropical zone and influenced by the Intertropical Convergence Zone (ITCZ), experiences high yearly rainfall. Coupled with diverse topography and geology, Indonesia is highly vulnerable to flash floods (Aldrian et al. 2005; Azmeri et al. 2016). In various parts of Indonesia, severe flash floods have resulted in extensive socio-economic losses, disrupted daily activities and caused loss of life. Although various flood susceptibility mapping methodologies are available, research that focuses on identifying the most appropriate statistical approach for the unique environmental context of Indonesia is still limited. This study aimed to evaluate the performance of three statistical methods, namely Shannon's Entropy (SE), Statistical Index (SI) and Frequency Ratio (FR), in assessing flash flood susceptibility. By integrating morphometric parameters and other conditioning factors such as elevation, slope, lithology, rainfall and land use, this study attempts to determine the most effective method for mapping flash flood susceptibility.

Materials and methods

Study area

The research area is located in the Upper Citarum Watershed, part of Cirata Watershed, and has an area of 220.19 km^2 with an altitude ranging from 269 to 2,979 m. The Upper Citarum Watershed

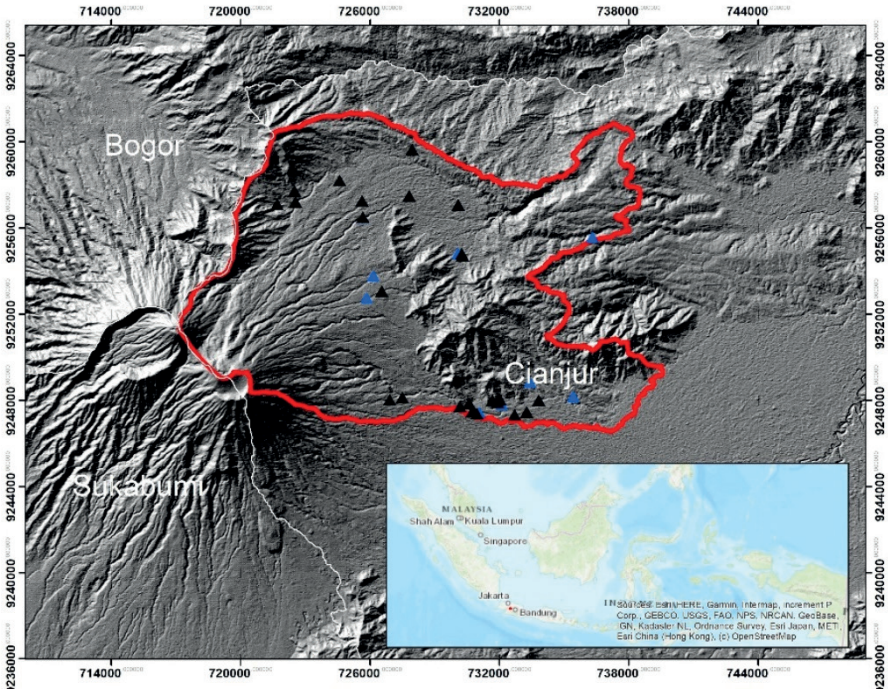

Fig. 1. Research area, the Upper Citarum Watershed, Indonesia

is located at 6°43'–7°15'N and 107°30'–108°E. It is bordered by Purwakarta and Subang Regencies to the north, Cianjur and Garut Regencies to the south, Bandung Regency to the west, and Sumedang and Garut Regencies to the east. The Citarum watershed has three significant reservoirs: Saguling, Cirata and Jatiluhur. The Upper Citarum Watershed is the water source for the Cianjur Regency area, as shown in Figure 1. Cianjur Regency of West Java has an area of 26.15 km^2 with a population density of 6,667 people/km^2, and is thus an area with high population density (Central Bureau of Statistics – BPS] of Cianjur Regency 2022). Geographically, the Cianjur Regency is divided into three parts, namely Northern Cianjur, located at the foot of Mount Gede with an altitude of 2,962 meters and a combination of mountainous topography, plantations and rice fields; Central Cianjur, an area with small hills; and Southern Cianjur, a lowland interspersed with small hills and mountains extending to the Indonesian Ocean.

Data

Figure 2(a) shows the land use/land cover (LULC) in the research area is forest area with 63.48 km^2 or 28.83% of the total area, followed by paddy fields of 47.19 km^2 (21.44%), settlements of 37.80 km^2 (17.17%), mixed plantation of 26.42 km^2 (12.01%), dry fields/fields of 22.37 km^2 (10.16%), shrubs of 3.49 km^2 (1.58%), rivers of 0.38 km^2 (0.17%), open land of 0.06 km^2 (0.03%), and ponds of 0.05 km^2 (0.02%) (Department of Public Works and Spatial Planning Cianjur 2022). Land cover in the Upper Citarum Watershed from 1990 to 2016 underwent changes predominantly characterized by increased shares for urban development, dryland agriculture and plantations. Meanwhile, the area covered by primary and secondary forests, mixed forests, orchards and rice fields decreased compared to previous years (Yulianto et al. 2020). Changes in forest cover area are one of the anthropogenic factors that can affect the rise and fall of surface flow discharge values, which in turn causes the spread of floods in the Upper Citarum sub-watershed (Dasanto et al. 2014).

The soil types in the study area consist of andosol, latosol and regosol (Department of Food Crops and Horticulture West Java 2024), as illustrated in Figure 2(b). Andosol soil is formed by parent materials like tuff and intermediate volcanic ash, predominantly found in hilly and mountainous regions at relatively high elevations. It has a deep profile, is rich in organic matter, features rapid drainage, and has high permeability (FAO 2015). Latosol soil has the largest area in the study area of 111.16 km^2. Latosol soil, which has low permeability,

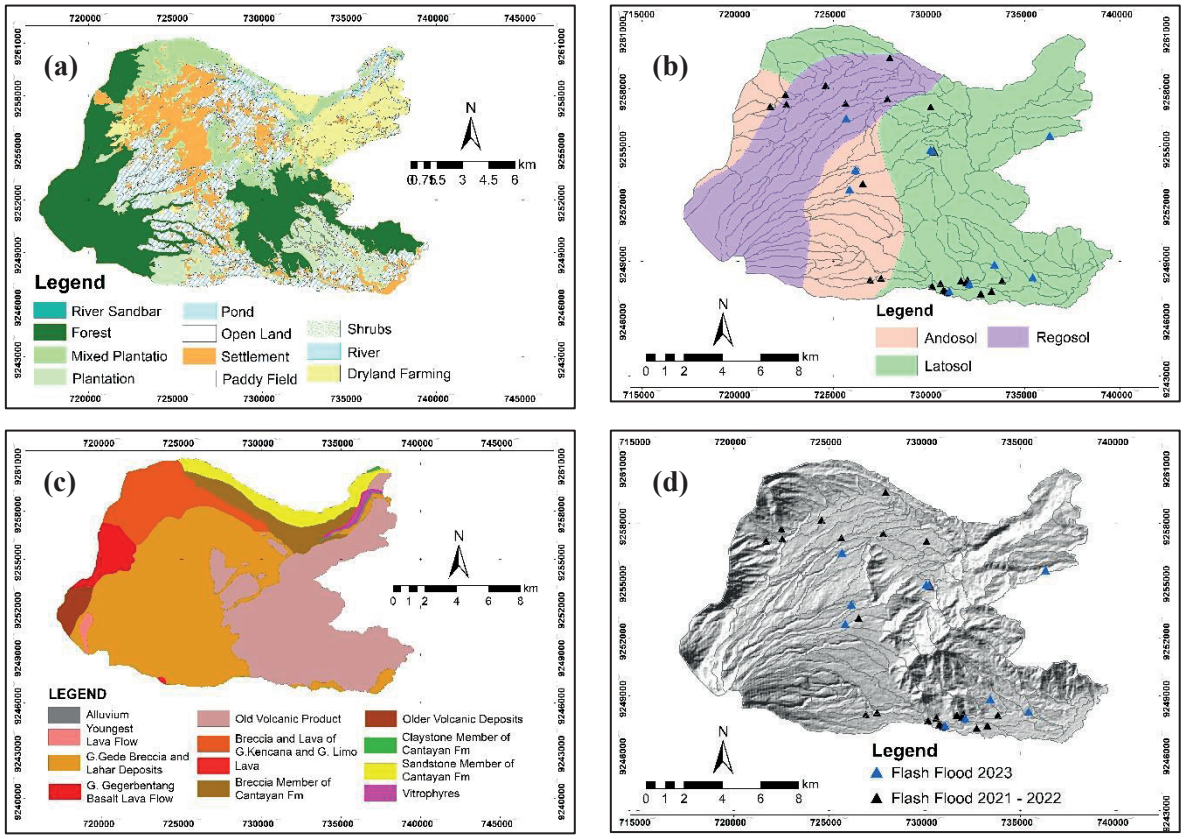

Fig. 2. Data input for Flash Flood Susceptibility Map
(a) LULC; (b) Soil type; (c) Geological data; (d) Flood events in 2021–2023

is very susceptible to erosion and can be easily eroded by rainfall. Regosol soil is spread in mountainous areas with an area of 65.63% (Chaidar et al. 2017).

The study area consists of twelve rock formations dominated by igneous and sedimentary rocks from past volcanic activity, as demonstrated in Fig. 2(c). There are Alluvium, Old Volcanic Product, G. Gegerbentang Basalt Lava Flow, Youngest Lava Flow, Breccia and Lava of G. Kencana and G. Limo, Older Volcanic Deposits, G. Gede Breccia and Lahar Deposits, Lava, Breccia Member of Cantayan Fm, Claystone Member of Cantayan Fm, Sandstone Member of Cantayan Fm, and Vitrophyres (Sudjatmiko 2003). G.Gede Breccia and Lahar Deposits Formation is the largest area, with 40.71% of all areas that consist of tuffaceous sandstone, shale, breccia and conglomerate. This formation also formed the Cianjur Plain (Sudjatmiko 2003).

Flooding in the Upper Citarum Watershed is one of the flood events in Indonesia that causes significant damage and losses. In 2021–1023, flash flood events occurred several times in many areas of Cianjur Regency. Flash floods and landslides in the Upper Citarum Watershed on March 20, 2023 caused seven sub-districts to be affected by flash floods and landslides. In addition, the disaster also caused losses in the form of damage to many paddy fields, roads, bridges, public facilities and worship facilities (National Agency for Disaster Countermeasure 2023). Poor management of the Citarum watershed has led to high levels of erosion, surface runoff, flooding, landslides, drought and pollution occurring in the watershed area.

Historical flash flood data are used as the basis for this study. Data-driven approaches are common and popular approaches used to predict the characteristics and locations of flash flood events, using statistical analysis and machine learning. The quality of research results is determined by the amount of historical data available; the more data available, the better the results (Wang et al. 2023). This research used historical data for 2021–2023 as shown in Figure 2(d) from the National Agency for Disaster Countermeasure and The Local Agency for Disaster Countermeasure Cianjur Regency. There are 25 (70%) historical flash flood events used for

analysis starting from 2021–2022, and ten (30%) flash flood events data from 2023 are used for validation. Google Earth Pro software is also used to validate the coordinate location of flash flood events.

Methods

The selection of flood-causing factors, known as conditioning factors, is the most influential stage in developing the final flood vulnerability map and has the most influence on the accuracy of the output map (Kia et al. 2012). Although there is still no framework or agreement on how to select flood conditioning factors, the most relevant and frequently used flood conditioning factors by other researchers were used in this study (Rahmati et al. 2016; Taherizadeh et al. 2023). The driving factors for flash floods can also be determined by analyzing hydrological and hydrodynamic processes in the watershed (Wang et al. 2023). The flood conditioning factor dataset was compiled using a digital elevation model (DEM), slope, curve number, lithology, soil movement, rainfall and watershed morphometric parameters. Figure 3 shows the methodological flow chart of this research.

DEM data were obtained by DEMNAS with 8.33 m resolution, which was used in this research for generated sub-watershed, morphometric analysis and slope analysis, and it was used for elevation factors in the susceptibility map. The elevation parameter in research is generated by dividing the DEM into five classes equally, as illustrated in Figure 4(a). The topographic factor, slope, has a considerable impact on the occurrence of floods (Pradhan 2009).

Steep slopes increase the speed of surface runoff and reduce the time available for the soil to absorb water. In terms of aspect factors, this parameter impacts the rainfall received and the amount of sunlight received by an area (Jebur et al. 2014). The slope factor generated from the DEM using spatial analysis in the Arc GIS 10.3 and divided into six classes based on modified classes from the United States Department of Agriculture (USDA) (Philip Schoeneberger et al. 2017). The research area is dominated by 8–15% slope. This slope class covers an area of 49.01 km^2 or 22.49% of the entire research area (Fig. 4b).

Sub-watersheds in the research area were processed using ArcGIS 10.3; then, morphometric analysis was carried out on each sub-watershed. Morphometric classification map is used as one parameter for the susceptibility map. Morphometric

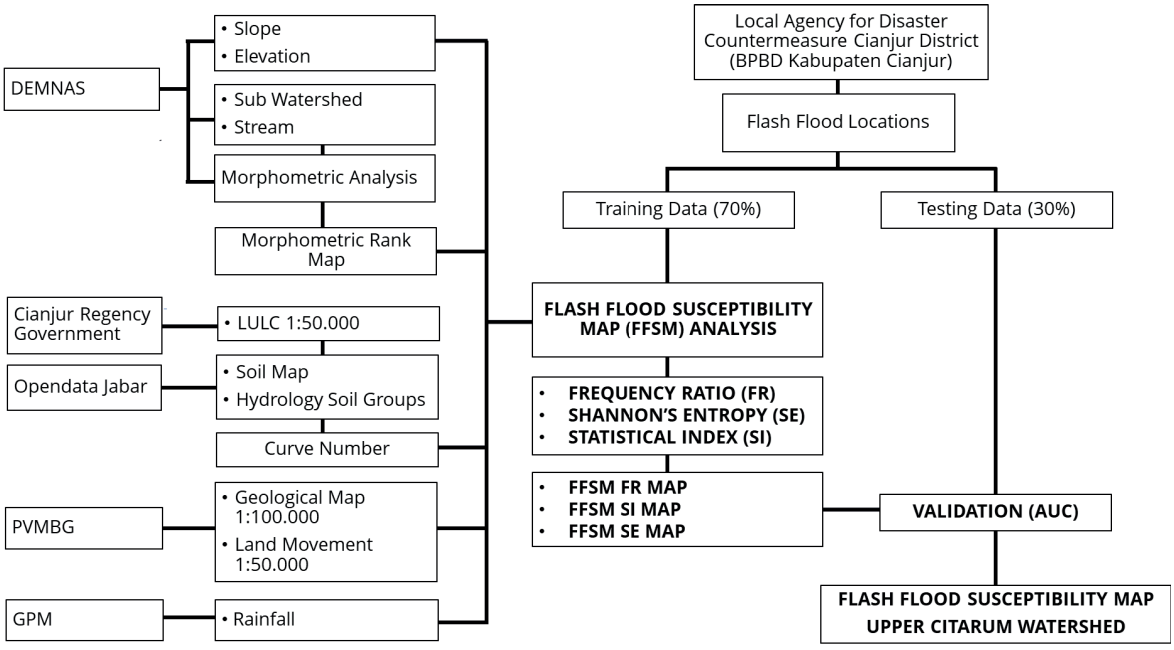

Fig. 3. Research flowchart, divided into three methods

parameters are used to determine the characteristics of sub-watersheds and the response of a watershed to flash floods. Morphometric parameter characteristics impact the hydrological processes of a watershed like surface runoff, soil erosion and sediment transport. It is important to understand the morphometric characteristics and their control on the pattern of a watershed to reduce the risk of flash flood hazards within an area (Elsadek and Almaliki 2024). Morphometrics parameters that have direct and inverse influence on hydrologic watersheds are listed in Table 1. The highest value has the highest

Table 1. Morphometric parameters for linear, shape and relief aspect

No	Morphometric Parameters	Formula	References
Linear aspect			
1	Area (A)	km^2	
2	Perimeter	km	
3	Stream order	U	(Strahler 1957)
4	Stream number	N_u = Total number of streams of all order in the watershed	(Strahler 1957)
5	Stream length	L_u	(Horton 1945)
6	Mean stream length	$L_{sm} = L_u/N_u$	(Strahler 1957)
7	Stream length ratio	$R_L = L_u/(L_{u-1})$	(Bagwan & Gavali 2021)
8	Stream frequency	$F_s = \Sigma N_u/A$	(Horton 1945)
9	Bifurcation ratio	$R_f = N_u/N_u+1$	(Schumm 1956)
10	Mean bifurcation ratio	R_{bm} = *Average of* R_b	(Strahler 1957)
11	Length of overland flow	$L_o = 1/(2D_d)$	(Smith 1950)
12	Basin length	$L_b = 1.312 \times A0.568$	(Bagwan & Gavali 2021)
13	Rho coefficient	$\rho = R_l/R_f$	(Horton 1945)
14	Constant of channel maintenance	$C = 1/Dd$	(Schumm 1956)
15	Drainage density	$D_d = L_u/A$	(Horton 1945)
16	Drainage texture	$T = D_d \times F_s$	(Horton 1945)
17	Texture ratio	$T_r = \Sigma N_u/P$	(Horton 1945)
Shape aspect			
1	Basin shape	$B_s = Lb^2/A$	(Javed et al. 2011)
2	Circularity ratio	$R_c = 4\pi A/P^2$	(Miller 1953)
3	Compactness coefficient	$C_c = 0.2821 \times P/A0.5$	(Horton 1945)
4	Elongation ratio	$R_e = 2\ (A/\pi)/Lb$	(Schumm 1956)
5	Form factor	$F_f = A/L^2$	(Horton 1945)
Relief aspect			
1	Basin relief	$R_h = H–h$	(Schumm 1956)
2	Relief ratio	$R_r = R_h/L_b$	(Schumm 1956)
3	Ruggedness number	$R_n = D_d \times B_h$	(Strahler 1957)
4	Melton ruggedness number	$MR_n = H–h/A0.5$	(Melton 1965)

Citation: Bulletin of Geography. Physical Geography Series 2024, 27, http://doi.org/10.12775/bgeo-2024-0012

rank and vice versa. Meanwhile, the lowest value in this parameter has the highest rank and vice versa (Dutal 2023).

There are three morphometrics parameters used in this research, such as linear parameters, shape parameters and relief parameters. Each parameter can be seen in Table 1. Morphometric characteristics such as area, perimeter, stream, stream order, stream number and stream length are generated with ArcGIS 10.3. All of the parameters are calculated by formulas in Table 1. After calculation, each parameter in morphometrics was sorted and ranked from highest to lowest for linear and relief parameters except for the length of overland flow and vice versa for shape parameters. Rank values from 1 to 126 were divided into five classes.

The curve number (CN) parameter was processed in ArcGIS 10.3 by soil map data at a scale of 1:250,000 from West Java Provincial Government website and LULC map from West Java Province Government at a scale of 1:50,000. Curve number is an empirical surface runoff method developed by the Natural Resources Conservation Service (NRCS) of USDA, formerly called the Soil Conservation Service (SCS). The SCS CN method estimates excess rainfall as a function of cumulative rainfall depth, soil cover, land use and soil moisture. Curve number values in the research area are divided into six CN classes, dominated by CN values in the range 71–80 accounting for 52.23% of area from all research areas.

The geology data used in this research were obtained from the Geological Map at a 1:100,000 scale from the Ministry of Energy and Mineral Resources website. Classification of igneous and sedimentary rocks is based on rock classification standards (Travis 1955; Streckeisen 1967; Pettijohn 1975). Twelve rock formations in the research area were reclassified into five classes based on the number of flash flood events found in each formation, with the highest number of flash flood events being the highest class. The formation with

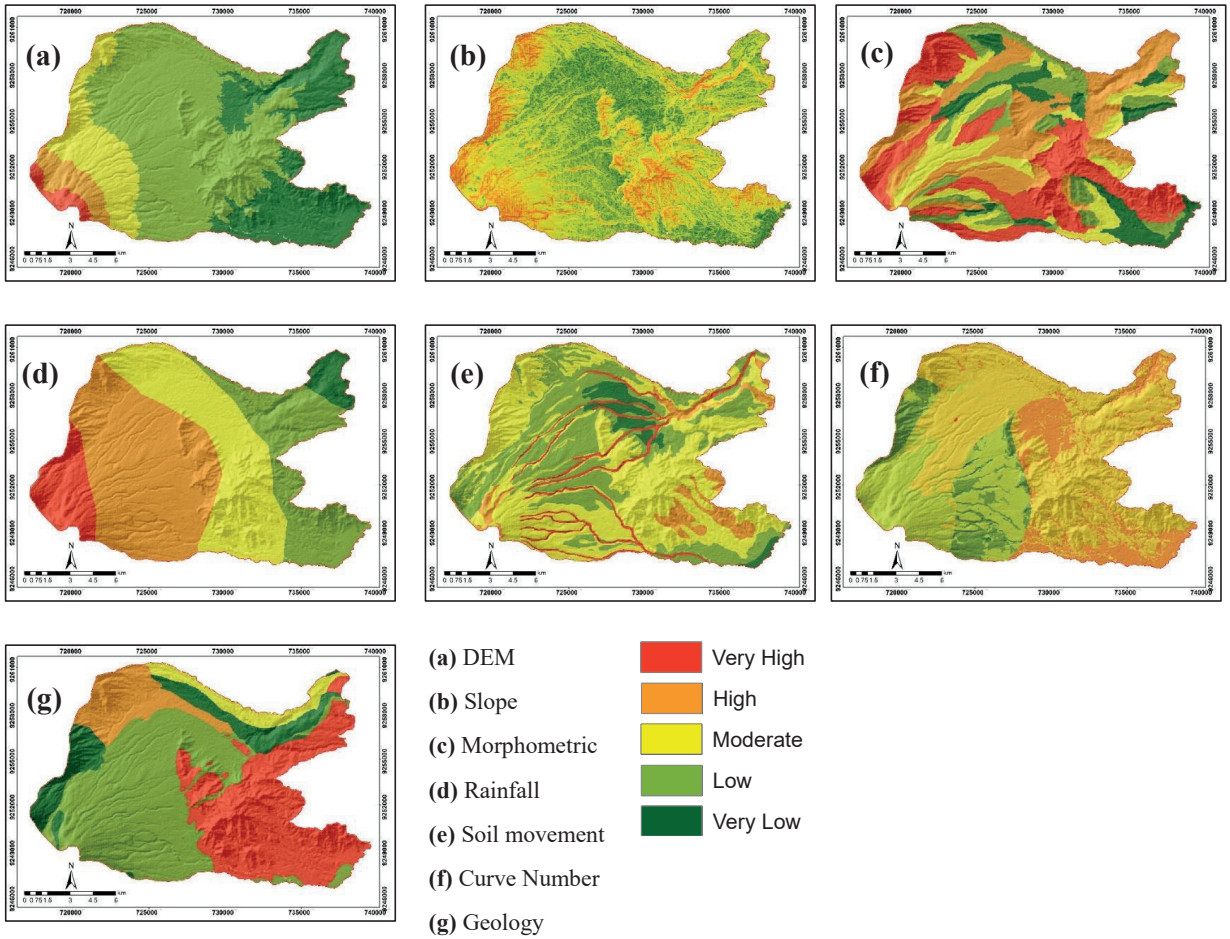

Fig. 4. Parameters for susceptibility map

the most flash flood events is the Oldest Volcanic Products, which consists of breccia and lava. Breccia with a composition of pyroxene andesite intercalated with andesitic lava. This formation is commonly propylitized, surrounded by Breccia and Lahar Deposits from G. Gede, and formed large isolated hilly hills (Sudjatmiko 2003).

The soil movement map used in this research was obtained from the Land Susceptibility Map at a 1:50,000 scale from the Center for Volcanology and Geological Disaster Mitigation (PVMBG), Ministry of Energy and Mineral Resources. The research area is divided into five classes based on the map: very low, low, moderate, high, and very high. The soil movement parameter in determining flood vulnerability is the movement of slope-forming material (soil, rock, fill material, or a mixture thereof) down and out of the slope (Cruden and Varnes 1993).

Rainfall data are obtained from satellite images generated by NASA's Global Precipitation Measurement (GPM) – Daily accumulated precipitation (combined microwave-IR) estimate – Final Run daily 0.1 deg. [GPM GPM_3IMERGDF v06] mm. The rainfall data in the research area is the average hourly rainfall for one year (2022). These rainfall data were analyzed with the IDW method in ArcGIS 10.3 and divided into five classes equally.

All parameters mentioned above were generated in raster format with a pixel size of 30 m × 30 m. It is important to utilize fast, easy-to-understand and accurate methods for flash flood modeling. Statistical methods do not have specific requirements regarding input data, software, computer capacity, and so on. Bivariate Statistic Analysis (BSA) methods, such as FR, SI and SE evaluate the impact of each class of each conditioning factor on flood occurrence (Khosravi et al. 2016; Samanta et al. 2018; Sarkar and Mondal 2020).

Frequency Ratio model

The Frequency Ratio (FR) method is end-user-friendly due to its simplicity and accuracy, and it can calculate each factor class based on the vulnerability ratio value of a flood (Mansour et al. 2024). Frequency Ratio is a simple bivariate statistical analysis that is often used for various types of disaster maps, such as floods, flash floods, landslides, erosion and other mapping, such as groundwater and mineral potential (Cao et al. 2016; Tehrany et al. 2019). The ability to understand the input, calculation and output procedures and the ease of implementation in environmental GIS environments makes the frequency ratio method an acceptable simplifier for vulnerability assessment when sufficient data are available (Li et al. 2017). Bonham-Carter, in 1994, first introduced the FR technique to represent the occurrence of certain features. In the FR model, a class with a higher value indicates a greater potential of that class for the occurrence of an event (such as flash floods, landslides, or groundwater potential). The context in this study indicates that a place is more susceptible to artificial recharge through the Flash Flood Susceptibility Map (FFSM). The FR can be calculated as follows:

$$FR = \frac{A/B}{M/N}$$

where *FR* is the ratio value, A is the number of pixels with flash flood location points in each parameter, B is the total number of pixels with flash flood location points, M is the number of pixels in each class in each parameter and N is the total number of pixels in the research area. After determining the FR value for each parameter, spatial analysis in ArcGIS 10.3 was carried out using the Spatial Analyst tool and Weighted Sum to create an FFSM FR map (Cao et al. 2016; Li et al. 2017; Tehrany et al. 2019).

Statistical Index model

The Statistical Index (SI) bivariate statistical method was introduced for landslide vulnerability mapping (Van Westen 1997). This method requires selecting and mapping important parameters and their classification into relevant classes, mapping the flood inventory, overlaying the flood inventory map with each causal factor, determining flood density in each parameter class, and calculating weight values.

Statistical Index is one of the least-used methods in natural hazard modeling and has never been tested in flood vulnerability mapping. The procedure for this method is fast and fairly simple, making it suitable for natural hazard modeling (Cao et al. 2016). The SI weight can be described as the

natural logarithm of the presence of flooding in each conditioning factor class divided by the total flood density in the study area (Bourenane et al. 2015). The equation used to calculate the SI weight (W_{ij}) (Cao et al. 2016) for each factor is as follows:

$$W_{ij} = In\left(\frac{D_{ij}}{D}\right) = \text{In}\left[\left(\frac{N_{ij}}{S_{ij}} / \frac{N}{S}\right)\right]$$

where the weight received for class i of conditioning factor j is given by W_{ij}; the flood density in class i of conditioning factor j is given by D_{ij}; the total flooding within the study area is given by D; the number of pixels with flooding in class i of conditioning factor j is given by N_{ij}; the total number of pixels in class i of conditioning factor j is given by S_{ij}; and N and S are, respectively, the total number of flooding and the total number of pixels across the study area (Cao et al. 2016).

After that, each factor was reclassified using the W_{ij} values obtained in ArcGIS 10.3 using the Spatial Analyst tool. The reclassified factors were added using a raster calculator to generate a flood probability index. This method is based on the statistical correlation between flood inventory maps and the characteristics of various parameters (Yalcin 2008). Flood vulnerability mapping is done by overlaying different layers. A positive W_{ij} value indicates a good and strong relationship between the flood class and distribution, so the stronger the relationship, the higher the resulting value. A negative value for W_{ij} means no relationship exists between class and flood occurrence (Cao et al. 2016; Tehrany et al. 2019).

Shannon's Entropy model

The Shannon's Entropy (SE) analysis was first expressed by Stephan Boltzmann, and then presented quantitatively by Shannon (1948) (Arora et al. 2021; Islam et al. 2022). The weight of the SE value can indicate which parameters have the most influence on flash floods. The weight of the entropy value can be calculated using the following equation (Arora et al. 2021; Hang et al. 2021; Islam et al. 2022):

$$P_{ij} = \frac{(B/A)}{\sum_{j=1}^{n} B/A}$$

$$E_j = -\frac{1}{ln ln\,(n)} \sum_{j=1}^{n} P_{ij}\, ln\,(P_{ij})$$

$$D_j = 1 - E_j,\ j = 1, 2, \ldots, n$$

$$W_j = \frac{D_j}{\sum_{j=1}^{n} D_j}$$

Accuracy assessment

This study used the Area Under the Curve (AUC) method to evaluate the efficiency and reliability of three flood probability maps derived from the FR, SI and SE methods (Tehrany et al. 2013). The AUC method is widely used in natural hazard studies because it is comprehensive and reasonable and an easy-to-understand validation method (Tehrany et al. 2019). In the FFPI class, the relative distribution of training and validation areas is the first method used for result validation and model performance assessment. The relative distribution in the training area is used to assess model performance, while the validation area is used for result validation. This method is widely used in studies on the assessment of vulnerability to various natural hazards (Hong et al. 2018).

This method starts by arranging the flood probability indices in descending order. Then, the compiled flood probability index is represented on the y-axis as sensitivity and the x-axis as specificity. This is followed by overlaying the flood inventory on the flood probability index. The presence of flood points (training and testing) in each class is evaluated, and predictions and success rates are obtained. Success rate and prediction are two products of the AUC technique. The training and testing flood datasets are used to generate success rates and predictions. AUC produces a range from zero to one. The method is 100% successful if the index value (or area under the curve) is equal to 1, indicating a full model fit; a value equal to 0.5 indicates a lack of model fit (Mansour et al. 2024). The training data, using the 2021–2022 flash flood location data of 25 location points, were used to analyze the success rate of ROC/AUC. A total of ten flash flood location points of 2023 data were used to analyze the validation (testing) of ROC/AUC. The success rate curve was used to analyze the model's ability, and the prediction rate indicates the ability of the model to develop flash flood mapping (Khosravi et al. 2016). Statistical evaluation measures of overall accuracy, specificity, sensitivity, positive predictive value (PPV) and negative

predictive value (NPV) were applied to measure the comparative performance of the models (Bui et al. 2011). Overall accuracy, sensitivity and specificity measure the proportion of training and testing, flooded and non-flooded samples that are correctly classified. PPV and NPV estimate the probability of training and testing dataset samples being correctly classified into the flooded class and non-flooded class, respectively.

$$Overall\ accuracy = \frac{TP+TN}{TP+TN+FP+FN},$$

$$Specificity = \frac{TN}{FP+TN},$$

$$Sensitivity = \frac{TP}{TP+FN},$$

$$PPV = \frac{TP}{FP+TP},$$

$$\mathrm{NPV} = \frac{TN}{FN+TN},$$

where True Positive (*TP*) and True Negative (*TN*) are the number of samples in the training and validation datasets, which are correctly classified into the flood and non-flood classes, respectively. False Positive (*FP*) and False Negative (*FN*) are the number of samples in the training and validation datasets that were incorrectly classified.

Results and discussion

Morphometric analysis

The value from each morphometrics parameter is presented in Figures 5 and 6. Linear parameters used in this research were basin area (*A*), perimeter (*P*), stream order (*u*), stream number (*Nu*), stream length (*Lu*), mean stream length (*Lsm*), stream length ratio (*RL*), stream frequency (*Fs*), bifurcation ratio (*Rb*), mean bifurcation ratio (*Rbm*), length of overland flow (*Lo*), rho coefficient (ρ), constant of channel maintenance (*C*), drainage density (*Dd*) and drainage texture (*T*). The Upper Citarum watershed has 218.07 km^2 of basin area and 1231.70 km perimeter. SB 125 has the highest value for many parameters, such as basin area, perimeter and stream length. SB 124 has the lowest value for parameters basin area, perimeter, stream order, stream length, mean stream length and drainage density. SB 97 has the lowest value for Lo.

Basin shape (*BS*), circularity ratio (*Rc*), compactness coefficient (*Cc*), form factor (*Ff*), and elongation ratio (*Re*) were used to shape parameters in this research area. The lowest value in this parameter has the highest rank and vice versa. SB119 has the highest rank for Rc and Cc parameters. SB94 has the highest rank for the Ff and Re parameters, while SB45 has the highest rank for the BS parameter.

In the relief parameter, the highest value has the highest rank and vice versa. The relief parameters used in this research are basin relief (*Rh*), relief ratio (*Rr*), ruggedness number (*Rn*), and Melton ruggedness number (*MRn*). SB119 has the highest rank for *Rc* and *Cc* parameters. SB61 has the highest rank for the *Rr* and *MRn* parameters, while SB43 has the highest rank for the *Rh* parameter and SB49 has the highest rank for the *Rn* parameter.

The value of morphometric from each SB was then summed and ranked from 1 to 126. The ranking of 126 is the highest value and has more potential risk for flash flood. All the ranks were divided into five classes and analyzed for each method. Each class has 24–26 sub-watersheds. The highest class range from morphometric parameters are from ranks 102–126. The sub-watersheds with the highest class are SB44, SB99, SB105, SB31, SB100, SB2, SB24, SB25, SB90, SB95, SB28, SB29, SB6, SB36, SB66, SB59, SB38, SB11, SB50, SB60, SB5, SB52, SB48, SB88, SB55 and SB57, as illustrated in Fig. 7.

Shannon's Entropy

Shannon's entropy analysis results related to flash floods are shown in Table 2. The highest score for all parameters is elevation, followed by landslide, rainfall, slope, morphometry, geology and curve number, with scores of 5.63, 4.32, 1.47, 0.59, 0.56, 0.37 and 0.34, respectively. These scores showed that the elevation parameter is the most influential parameter on flash flood events in the research area, based on this method, followed by landslide and rainfall parameters. Shannon's Entropy Susceptibility Map was generated based on the score of each parameter, as displayed in Figure 8. There are five disaster levels from very low, low, medium, high, to very high. The high and very high classes have an area of 69.28 km^2 and 8.57 km^2 or 31.80% and 3.93%, respectively. The class with the highest area is the moderate class with an area of 114.70 km^2 or 52.64% of the total area of the Upper Citarum Watershed.

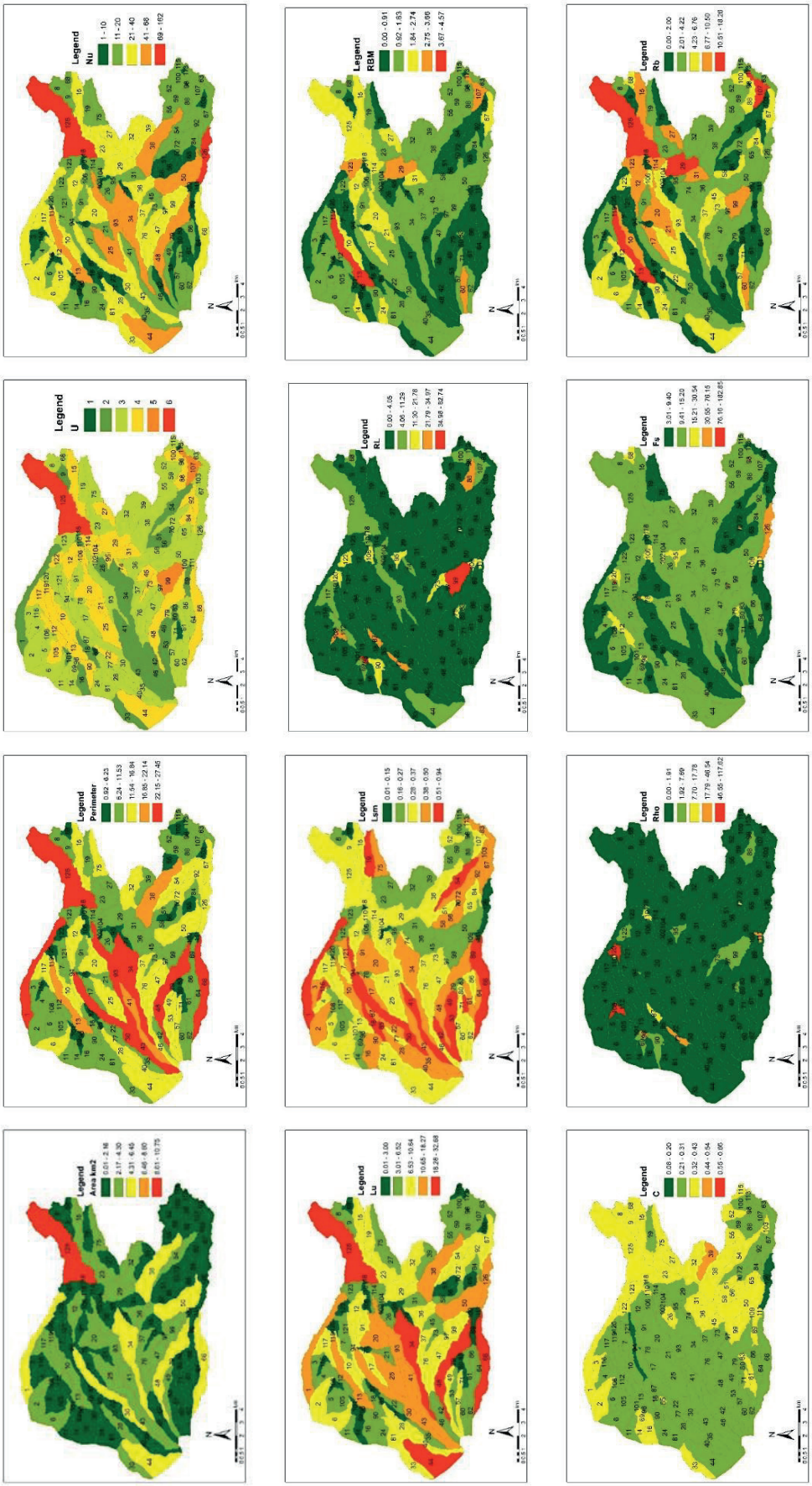

Fig. 5. Morphometric analysis (A, P, U, Nu, Lu, Lsm, RL, RBM, C, , Fs, Rb)

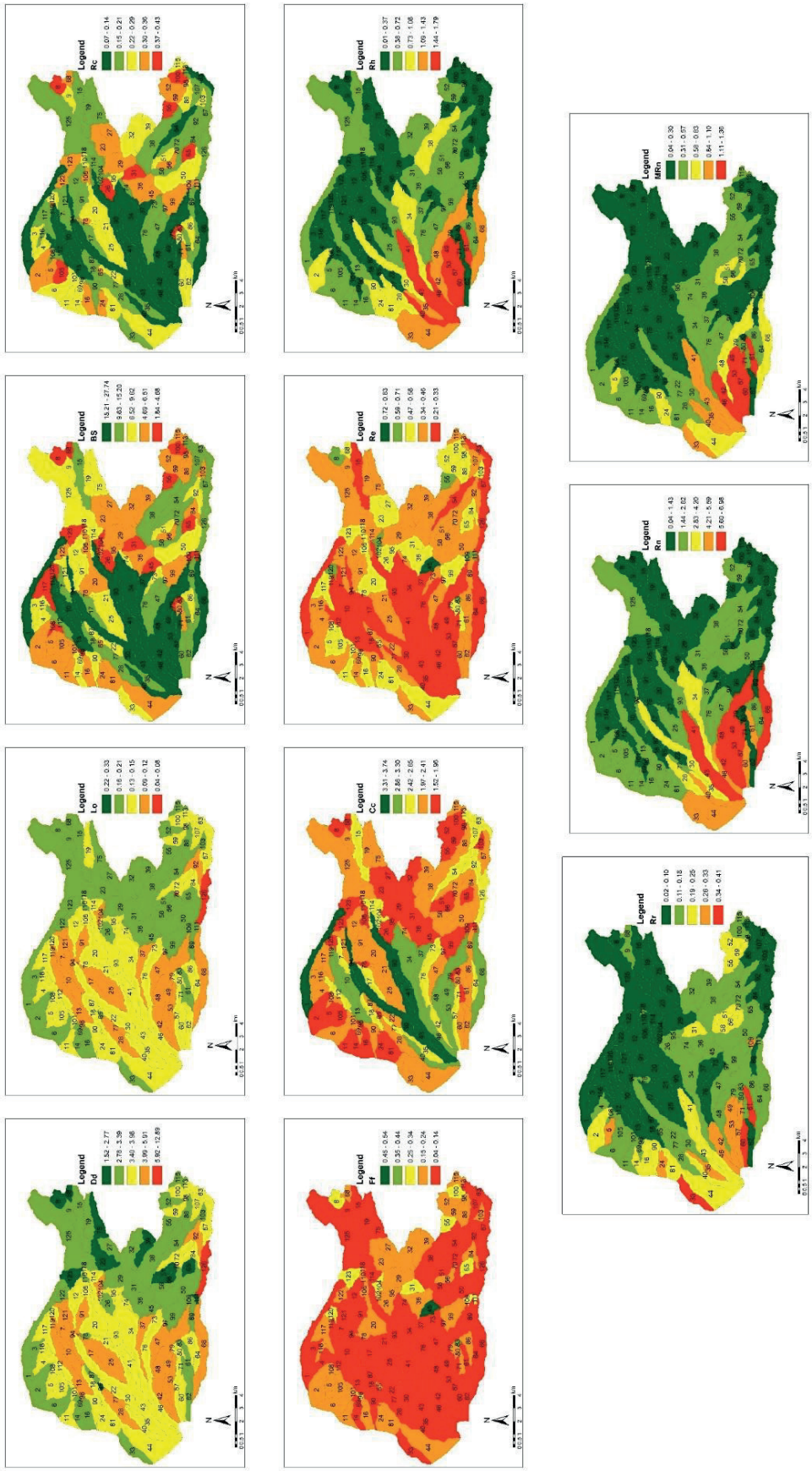

Fig. 6. Morphometric analysis (Dd, Lo, BS, Rc, Ff, Cc, Re, Rh, Rr, Rn, MRn)

Citation: Bulletin of Geography. Physical Geography Series 2024, 27, http://doi.org/10.12775/bgeo-2024-0012

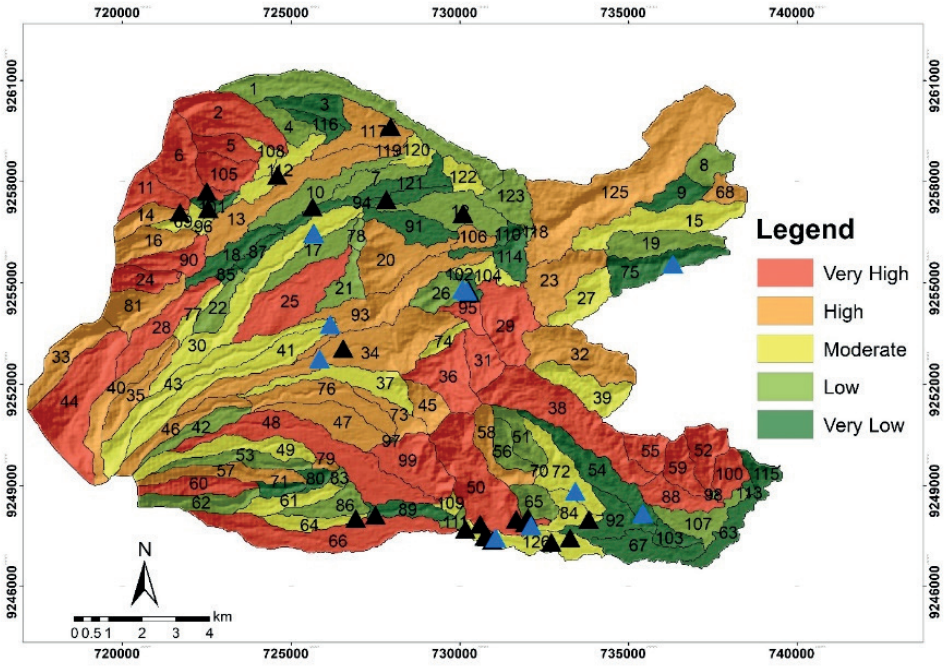

Fig. 7. Morphometric Rank Map

Statistical Index

The results of the Statistical Index analysis are shown in Table 2. In the SI method, there are positive and negative scores. A class with positive scores means that the class has a positive correlation with flash floods, while negative scores have no correlation with flash floods (Tehrany et al. 2019). A class with –2 scores indicates that no flash floods occurred in that class. In the elevation parameter, 269–811 has the highest score, at 2.45. This score indicates that the lower the elevation, the greater the potential for flash floods. In the slope parameter, the slope percentage classes that have positive scores are 0–3%, 3–8% and 8–15%, with scores of 0.66, 0.83 and 0.35, respectively. The highest score is on the gently undulating–undulating slope with a value of 3–8%. In the geology parameter, the classes with positive scores are the Old Volcanic Product Formation and Breccia and Lava of G. Kencana and G. Limo with scores of 0.29 and 0.70, respectively. The old volcanic product formation is Quaternary with lithology in the form of pyroxene andesite breccia and andesite lava. The Breccia and Lava Formation of G. Kencana and G. Limo consists of chunks of andesite breccia, andesite lava and andesite tuff (Sudjatmiko 2003). In the CN parameter, the SI with positive scores are in the CN 71–80 and 81–90 classes with scores of 0.20 and 0.08 respectively. In the hourly rainfall parameter, there is only one class with a positive score, that is 0.347–0.353 mm/hr class with score of 1.05. In the morphometric parameters of the ranking classes 1–26 and 77–101 have positive scores of 0.93 and 0.31. The SI Flash Flood Susceptibility Map is divided into five classes from very high to very low. The high and very high classes have an area of 93.06 km^2 and 9.23 km^2 or 42.71% and 4.24% respectively. The class with the highest area is the high class with an area of 93.06 km^2 or 42.71% of the total area of the Upper Citarum Watershed, as illustrated in Fig. 9.

Frequency Ratio

The results of the Frequency Ratio analysis related to flash floods are shown in Table 2. The higher the scores, the greater the influence of the parameter on the potential for flash floods. In the elevation parameter, 269–811 has the highest score, at 11.60. Similarly to the SI results, the potential for flash floods is greater at low elevations. In the slope parameter, the highest slope percentage class is 3–8% slope with a score of 2.30. In the geology parameter, the class with the highest score is the Breccia and Lava Formation of G. Kencana and G. Limo with a score of 1.34. In the CN parameter, the CN 71–

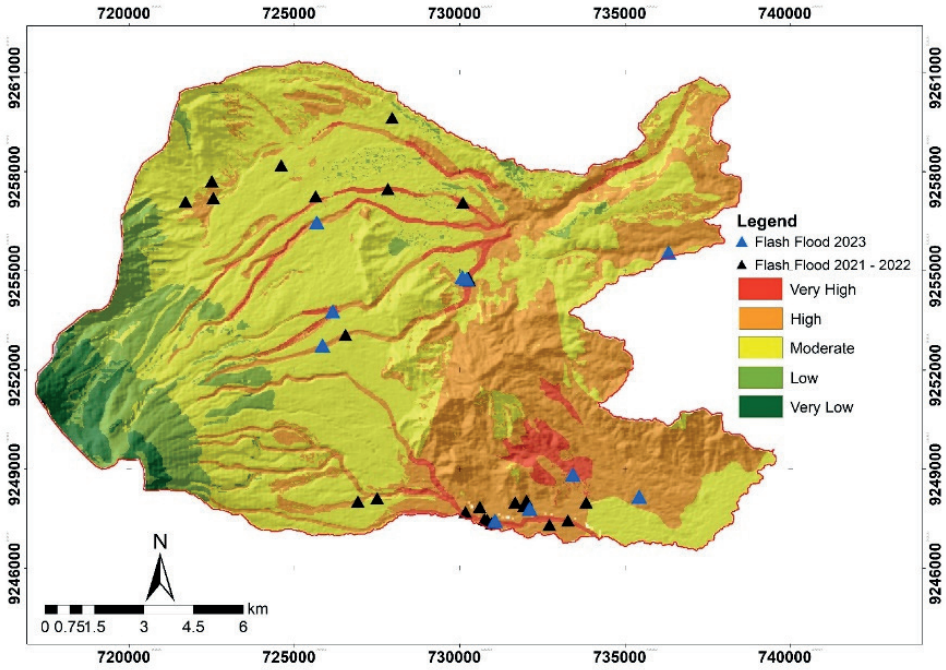

Fig. 8. Shannon's Entropy Flash Flood Susceptibility Map

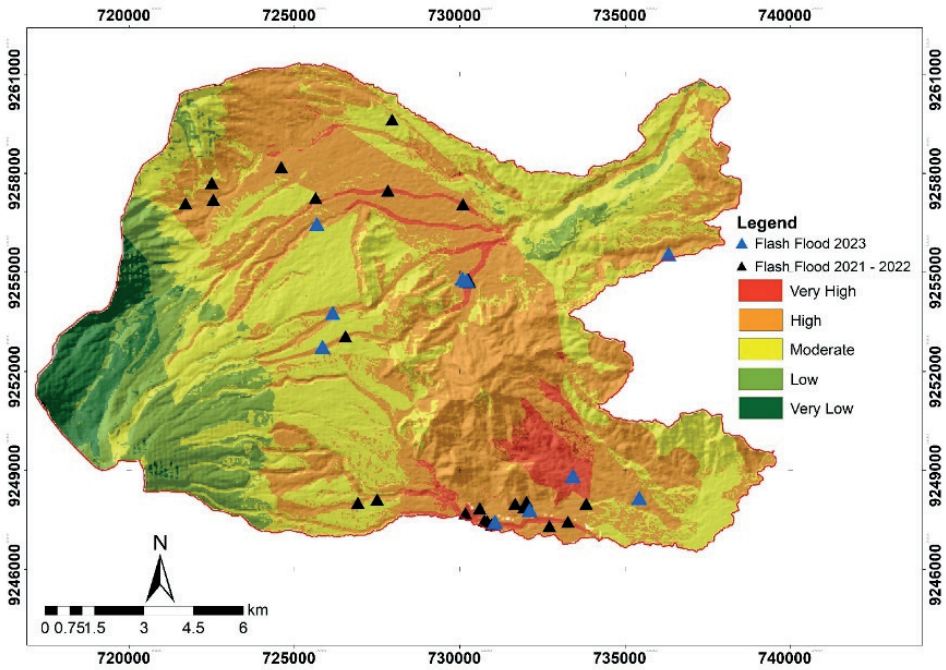

Fig. 9. Statistical Index Flash Flood Susceptibility Map

Citation: Bulletin of Geography. Physical Geography Series 2024, 27, http://doi.org/10.12775/bgeo-2024-0012

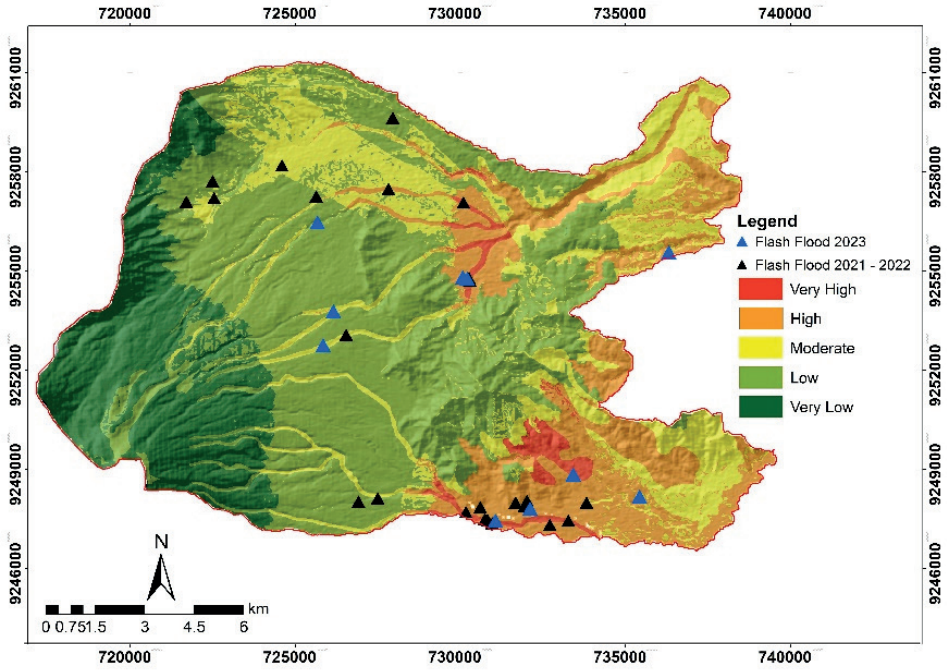

Fig. 10. Frequency Ratio Flash Flood Susceptibility Map

80 class has the highest score, at 1.23. In the hourly rainfall parameter, the class with the highest score is the 0.347–0.353 mm/hr class with a score of 2.85. In the morphometry parameter, the ranking class 1–26 has the highest score, atf 2.53. The FR flash floods susceptibility map in Figure 10 contains five classes from very high to very low. The high and very high classes have areas of 35.34 km^2 and 4.62 km^2 or 16.22% and 2.12%, respectively. The class with the highest area is the low class with an area of 96.24 km^2 or 44.17% of the total area of the Upper Citarum Watershed.

Validation

Model quality and model prediction accuracy were checked using ROC curves. Flood vulnerability maps for SI, FE and FR were validated through success ratio and prediction ratio curves as shown in Fig. 11. The success ratio results were obtained using a training dataset of 71.43% of flood locations (25 flood locations from 2021–2022). Prediction accuracy was calculated using a testing dataset of 28.57% of flood locations (10 flood locations in 2023). A value of 1.0 indicates the highest accuracy and that the model is fully capable of predicting an event without bias (Hong et al. 2018; Mansour et al. 2024). Therefore, an AUC value close to 1.0 indicates that the model is accurate and reliable (Bui et al. 2011; Hong et al. 2018; Mansour et al. 2024). In this study, the area under the curve (AUC) of the success rate of the SE, SI and FR models were 0.815, 0.907 and 0.794, respectively. The prediction level of each SE, SI and FR model has an AUC value of 0.902, 0.933 and 0.831, respectively. Of the three models, the SI model has the highest success rate and prediction rate, or closest to 1, at 0.907 and 0.933.

Discussion

Based on the AUC value, the SI FFSM has the best map model to represent flash flood susceptibility in the research area. The SI method showed the highest conformity with real conditions, achieving the highest AUC values for both success rate (0.907) and prediction rate (0.933). It makes the most suitable bivariate statistical method for using morphometric parameters in flash flood susceptibility assessment.

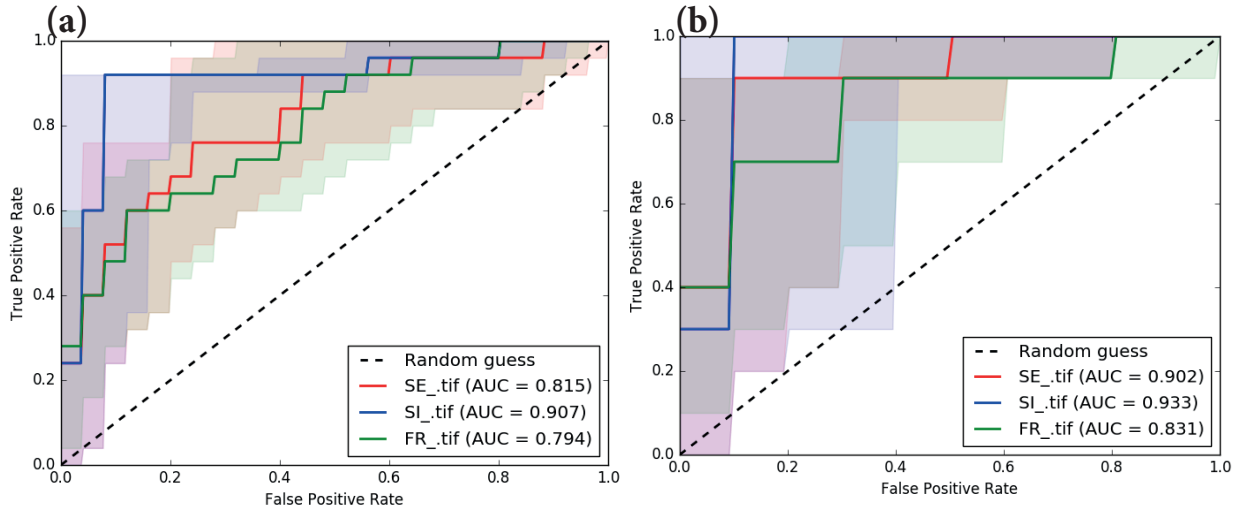

Fig. 11. Validation curve of Flash Flood Susceptibility Map in the Upper Citarum Watershed: (a) success rate curve; (b) prediction rate

The comparison between bivariate statistical methods in many previous studies showed the superiority of the SI method compared to other methods (Khosravi et al. 2016; Tehrany et al. 2019). This may be influenced by the parameters used, the area, the location of the watershed and the amount of data used. In addition, it is also influenced by the class division used. This study uses an "equal" class division or the same interval in each class, while in several studies the classes are divided based on the "natural breaks" method in each class (Cao et al. 2016). The number of classes is determined based on the availability of data and the parameters used in the study. In the FR method, the low accuracy is also likely due to its simple calculation procedure. FR is more applicable in linear feature mapping than in mapping complex and non-linear events such as flooding (Tehrany et al. 2019).

SI FFSM in this research was combined with morphometric analysis in 126 sub-watersheds. SB 126 has the most flash flood event points with seven event points, followed by SB50 with four event points. SB126 and SB50 are located on the high and very high classes in SI FFSM, as shown in Figure 9. SB 126 has the highest stream number value with 162, while SB50 also has a high class stream number value. Stream numbers are influenced by lithology, soil characteristics and rainfall. High stream numbers influenced the dynamics of river flow processes that occur in a short time (Dutal 2023; Mahmood and Rahman 2019). SB 97 has the highest Lo ranking with 0.04. SB126 also has a high-rank Lo with rank 123 (with a Lo value of 0.06). Lo refers to the distance water travels across the surface before converging into a stream channel. Higher values of this distance reduce surface runoff (Bagwan and Gavali 2021). A sub-watershed with a higher value of the linear parameters has a higher potential risk of flash floods, except for length overland flow, because the highest area of the watershed has the lowest length of overland flow. The size of the watershed affected the stream time concentration of runoff, which increased the risk of flash floods (Costache et al. 2020). SB 126 has a high rank (>100) for many linear morphometric parameters, including stream number (Nu), stream length (Lu), drainage density (Dd), stream frequency (Fs), length of overland flow (Lo), and drainage texture (T).

In the shape aspect, SB119 has the highest value for the circularity ratio. The form factor has an inverse relationship with the elongation ratio. Form factor values indicate high discharge with short duration; therefore, it can be a parameter to predict flow intensity in a watershed (Dutal 2023).

Basin relief parameters showed the geomorphological characteristics of the basin, flood patterns, and the amount of sediment volume that can be transported in a basin. Basins on very steep slopes have high flow velocities and short concentration times, causing higher flood peaks (Ogarekpe et al. 2022). Increasing basin relief and relief ratio values align with the level of flash flood hazard in a watershed (Mahmood and Rahman 2019). Model SB 43 has the highest value for basin relief and SB 61 has

Citation: Bulletin of Geography. Physical Geography Series 2024, 27, http://doi.org/10.12775/bgeo-2024-0012

Table 2. Results of Statistical Index, Shannon's Entropy and Frequency Ratio

III. Soil Movement													
No	**Classes**	**Area (pixel)**	**% of Area**	**No. of Flood**	**% of Floods**	**SI**	**FR**	***Pij***	**H*ij***	**H*j***	**H*jmax***	**I*j***	**W*j***
I. Elevation (m)													
1	269–811	45,071	18.41	14	56.00	2.45	11.60	0.73	0.33	0.83	2.32	1.78	5.63
2	812–1,353	98,052	40.06	11	44.00	1.43	4.19	0.27	0.51				
3	1,354–1,895	62,747	25.63	0	0.00	-2	0.00	0.00	0.00				
4	1,896–2,437	26,474	10.81	0	0.00	-2	0.00	0.00	0.00				
5	2,438–2,979	12,449	5.09	0	0.00	-2	0.00	0.00	0.00				
II. USDA													
1	0–3	5,021	2.07	1	4.00	0.66	1.93	0.26	0.00	1.83	3.00	0.64	0.59
2	3–8	29,480	12.17	7	28.00	0.83	2.30	0.31	0.52				
3	8–15	54,451	22.49	8	32.00	0.35	1.42	0.19	0.46				
4	15–30	78,113	32.26	5	20.00	-0.48	0.62	0.08	0.30				
5	30–45	41,684	17.21	3	12.00	-0.36	0.70	0.09	0.32				
6	45–65	25,349	10.47	1	4.00	-0.96	0.38	0.05	0.22				
7	65–140	8,064	3.33	0	0.00	-2	0.00	0.00	0.00				
8	>140	3	0.00	0	0.00	-2	0.00	0.00	0.00				
III. Geology													
1	Breccia Member of Cantayan Fm.	12,548	5.13	0	0.00	-2	0.00	0.00	0.00	1.89	3.58	0.90	0.37
2	Claystone Member of Cantayan Fm.	174	0.07	0	0.00	-2	0.00	0.00	0.00				
3	Sandstone Member of Cantayan Fm	11,923	4.88	1	4.00	-0.20	0.82	0.17	0.43				
4	Alluvium	655	0.27	0	0.00	-2	0.00	0.00	0.00				
5	Older Volcanic Deposits	80,324	32.84	11	44.00	0.29	1.34	0.27	0.51				
6	G. Gegerbentang Basalt Lava Flow	7,944	3.25	0	0.00	-2	0.00	0.00	0.00				
7	Youngest Lava Flow	1,252	0.51	0	0.00	-2	0.00	0.00	0.00				
8	Breccia and Lava of G. Kencana and G. Limo	24,220	9.90	5	20.00	0.70	2.02	0.41	0.53				
9	Older Volcanic Deposits	4,393	1.80	0	0.00	-2	0.00	0.00	0.00				
10	G. Gede Breccia and Lahar Deposits	99,554	40.71	8	32.00	-0.24	0.79	0.16	0.42				
11	Lava	162	0.07	0	0.00	-2	0.00	0.00	0.00				
12	Vitrophyres	1,416	0.58	0	0.00	-2	0.00	0.00	0.00				

IV. Soil Movement												
1	Very low	10,537	4.31	0	0.00	-2	0.00	0.00	0.00	0.77	2.32	2.03	4.32
2	Low	81,215	33.20	0	0.00	-2	0.00	0.00	0.00				
3	Moderate	120,872	49.41	8	32.00	-0.43	0.65	0.06	0.24				
4	High	18,000	7.36	8	32.00	1.47	4.35	0.39	0.53				
5	Very High	14,005	5.72	9	36.00	1.84	6.29	0.56	0.47				
V. Curve Number													
1	48–50	532	0.22	0	0.00	-2	0.00	0.00	0.00	1.50	2.58	0.73	0.34
2	51–60	21,433	8.76	2	8.00	-0.09	0.91	0.00	0.00				
3	61–70	58,076	23.75	3	12.00	-0.68	0.51	0.18	0.45				
4	71–80	127,744	52.23	16	64.00	0.20	1.23	0.44	0.52				
5	81–90	36,299	14.84	4	16.00	0.08	1.08	0.38	0.53				
VI. Average Hourly Rainfall 2022													
1	0.339–0.346	10,384	4.24	0	0.00	-2	0.00	0.00	0.00	0.78	2.32	1.99	1.47
2	0.347–0.353	53,647	21.91	0	0.00	-2	0.00	0.00	0.00				
3	0.347–0.353	58,477	23.88	17	68.00	1.05	2.85	0.77	0.29				
4	0.361–0.367	92,358	37.72	8	32.00	-0.16	0.85	0.23	0.49				
5	0.368–0.374	29,971	12.24	0	0.00	-2	0.00	0.00	0.00				
VII. Morphometric Ranking													
1	1–26	23,242	9.50	6	24.00	0.93	2.53	0.42	0.00	1.55	2.32	0.50	0.56
2	27–51	33,565	13.72	3	12.00	-0.13	0.87	0.13	0.39				
3	52–76	38,079	15.57	2	8.00	-0.67	0.51	0.11	0.34				
4	77–101	72,064	29.46	10	40.00	0.31	1.36	0.25	0.50				
5	102–126	77,678	31.75	4	16.00	-0.69	0.50	0.09	0.32				

the highest value for relief ratio. Areas with high flash flood potential have higher relief, drainage density and ruggedness number values. This indicates that sub-watersheds with high-risk flash flood potential have combinations of high ruggedness numbers with dense drainage, steep slopes and channel gradients. SB 49 has the highest value for Rn, while SB 61 has the highest value for MRn.

The combination of the reclassification results of the morphometric ranking map with the flash flood location map in Figure 7 shows that the moderate class has the most flash flood location points, compared to the very high and high classes, even the flash flood occurrence points in the very low class are more than the high class. SB 126, with seven flash flood locations, has a moderate rank morphometrics class; SB50, with four flash flood locations, has a high morphometrics rank; and SB44, with no flash flood event locations, has the highest rank and highest class. SB126 is also located in a high zone in SI FFSM. There are many different conditions between rank and flash flood susceptibility classes. In addition to morphometric parameters, other parameters affect flash flood disasters, such as elevation, slope, rainfall, soil and rock conditions, and vegetation in a watershed. SB44 is located near the peak of Mount Gede, so it is impossible for flash floods to occur in this area. Meanwhile, SB 126 is located in the lowest elevation range in the research area, at 269–811 m, so flash flood events have more possibility to occur in SB126. Morphometric analysis needs to be combined with other parameters and other methods so that the results of the flash flood disaster vulnerability map are close to reality.

The three parameters with the highest SI values (>1) in Table 2 are elevation, landslide and rainfall. The elevation parameter has the highest value in SI FFSM. This means that the elevation parameter has the most influence on flash flood disasters in the research area. Floods and flash floods generally occur at lower altitudes and are unlikely to occur on mountain peaks (Tehrany et al. 2013). The second parameter with a high value after elevation is soil movements or landslides. Flash floods and landslides often occur simultaneously and are caused by prolonged heavy rainfall on steep mountain slopes. Natural landslides formed in river valleys in mountainous areas are triggered by intense rainfall, which can cause flash floods or debris flows in a short time (Luu et al. 2023). The third parameter is the average hourly rainfall. Intensive rainfall triggered landslides and flash floods in river valleys on the mountain slopes. Dam failure is caused by increased runoff in the rivers and turned into flash floods with high sediment concentrations or debris flow (Luu et al. 2023).

Positive values in SI FFSM have a positive correlation with flash floods. Based on the SI analysis results in Table 2, flash floods in the research area occurred at elevations of 266–811 m in gently sloping to undulating areas with slope values of 3–8%. Flash floods in the research area were also influenced by the lithology of andesite breccia, andesite lava and andesite tuff rocks in the Breccia and Lava of G. Kencana and G. Limo formations and were in a very high landslide zone, with curve number values of 71–80 and average hourly rainfall values for one year of 0.347–0.353 mm/hour.

Moreover, climate change significantly impacts extreme rainfall and flash flood risk in Indonesia. Future events will likely exceed historical records in frequency and intensity, especially in densely populated areas such as Java (Kurniadi et al. 2024; Lubis and Respati 2021). The intensification of extreme rainfall events is expected to be more pronounced during the rainy season and in areas with higher baseline rainfall (Tabari 2020). Frequent heavy rainfall and unpredictable changes in rainfall patterns, such as erratic timing of the rainy season and uneven distribution of rainfall, increase the risk of flash floods. These changes disrupt the hydrological cycle, often causing prolonged droughts followed by heavy rains that flood drainage systems and infrastructure (Chen et al. 2023; Wang and Liu 2023).

In general, the SI method provides the best results for flash flood vulnerability maps in this area. Flash flood vulnerability maps can show predictions of the spatial mapping of flash flood events but cannot show information about the temporal probability of that disaster. This study used limited flash flood data (3 years) and low to medium spatial resolution. Therefore, further research can be carried out in more detail and incorporate the influence of climate change projections and land use changes so that flash flood disaster mitigation activities can be carried out more optimally.

Conclusion

The Upper Citarum watershed has experienced flash floods multiple times in various areas of Cianjur Regency. Mapping flash flood susceptibility areas to identify flash-flood-prone zones can be an effective mitigation tool. This study has identified the most suitable statistical method for using morphometric parameters in flash flood susceptibility assessment, including SE, SI and FR. The results showed that morphometric analysis identified 26 high-risk sub-watersheds like SB44 and SB99, while the SE method highlighted the high and very high areas, covering 35.73%. The SI method indicated that 42.71% of the area had high-risk susceptibility, while the FR identified 16.22% as high-risk. The validation results showed that the SI method produced conformity with actual conditions in the field, with the highest AUC value of success rate and prediction rate or closest to 1, which are 0.907 and 0.933. The three parameters that have the most influence on flash floods in the research area based on SI method are elevation, landslides or soil movement, and rainfall. The characteristics of flash floods in the research area based on the SI method are that they occur at low elevations with undulating to gentle slopes in very high landslide zones, with dominant andesite breccia rock lithology and rainfall of average hourly rainfall values for one year of 0.347–0.353 mm/hour. The characteristics of flash floods in the research area based on the SI method are low elevations with undulating to gentle slopes in very high landslide zones, with dominant andesite breccia rock lithology, and rainfall of average hourly rainfall values in 2022 of 0.347–0.353 mm/hour. The total area of high and very high flash flood susceptibility is 102.29 km^2, or 46.95% of the total research area. The disaster susceptibility map with the best results is expected to be used as a basis or reference for recommendations to the government to make disaster mitigation plans in the research area.

Acknowledgment

The authors would like to thank the Program House of Prototype Technology for Disaster Monitoring Hydrometeorology and Climate, Research Organization for Earth and Maritime, National Research and Innovation Agency (BRIN), for providing financial support for this study.

Disclosure statement

No potential conflict of interest was reported by the authors.

Author contributions

Study design: FW, ES, NW, MY, BS, WS, AP, ET, IR; data collection: NW, MY, ET; spatial analysis: AP, FW, ES; statistical analysis: FW, IR; result interpretation: BS, WS, IR; manuscript preparation: FW, ES, BS, WS; literature review: ET, NW, MY, AP.

References.

ALEKSOVA B, MILEVSKI I, MIJALOV R, MARKOVIĆ SB, CVETKOVIĆ VM and LUKIĆ T, 2024, Assessing risk-prone areas in the Kratovska Reka catchment (North Macedonia) by integrating advanced geospatial analytics and flash flood potential index. *Open Geosciences* 16(1): 20220684. DOI: DOI: https://doi.org/10.1515/geo-2022-0684.

ARORA A, PANDEY M, SIDDIQUI MA, HONG H and MISHRA VN, 2021, Spatial flood susceptibility prediction in Middle Ganga Plain: comparison of frequency ratio and Shannon's entropy models. *Geocarto International* 36(18): 2085–2116. DOI: https://doi.org/10.1080/10106049.2019.1687594.

AZMERI, HADIHARDAJA IK and VADIYA R, 2016, Identification of flash flood hazard zones in mountainous small watershed of Aceh Besar Regency, Aceh Province, Indonesia. *The Egyptian Journal of Remote Sensing and Space Sciences* 19(1): 143–160. DOI: https://doi.org/10.1016/j.ejrs.2015.11.001.

BAGWAN WA and GAVALI RS, 2021, An Integrated Approach for the Prioritization of Subwatersheds in the Urmodi River Catchment (India) for Soil Conservation using Morphometric and Land Use Land Cover (LULC)

factors. *Journal of Sedimentary Environments* 6(1): 39–56. DOI: https://doi.org/10.1007/s43217-020-00041-4.

BOURENANE H, BOUHADAD Y, GUETTOUCHE MS and BRAHAM M, 2015, GIS-based landslide susceptibility zonation using bivariate statistical and expert approaches in the city of Constantine (Northeast Algeria). *Bulletin of Engineering Geology and the Environment* 74(2): 337–355. DOI: https://doi.org/10.1007/s10064-014-0616-6.

BUI DT, LOFMAN O, REVHAUG I and DICK O, 2011, Landslide susceptibility analysis in the Hoa Binh province of Vietnam using statistical index and logistic regression. *Natural Hazards* 59(3): 1413–1444. DOI: https://doi.org/10.1007/s11069-011-9844-2.

CAO C, XU P, WANG Y, CHEN J, ZHENG L and NIU C, 2016, Flash flood hazard susceptibility mapping using frequency ratio and statistical index methods in coalmine subsidence areas. *Sustainability* (Switzerland): 8(9): 948. DOI: https://doi.org/10.3390/su8090948.

CEA L and COSTABILE P, 2022, Flood Risk in Urban Areas: Modelling, Management and Adaptation to Climate Change: A Review. *Hydrology*, 9(3): 50. DOI: https://doi.org/10.3390/hydrology9030050.

Central Bureau of Statistics (BPS) of Cianjur Regency, 2022, Cianjur Regency in Figures 2022. In: (E. Sulaeman E and Nugraha BDP (eds), BPS-Statistics of Cianjur Regency.

CHAIDAR AN, SOEKARNO I, WIYONO A and NUGROHO J, 2017, Spatial analysis of erosion and land criticality of the upstream Citarum watershed. *International Journal of Geomate* 13(37): 133–140. DOI: https://doi.org/10.21660/2017.37.34572.

CHEN J, SHI X, GU L, WU G, SU T, WANG H-M, KIM J-S, ZHANG L and XIONG L, 2023, Impacts of climate warming on global floods and their implication to current flood defense standards. *Journal of Hydrology* 618: 129236. DOI: https://doi.org/10.1016/j.jhydrol.2023.129236.

COSTACHE R, HONG H and PHAM QB, 2020, Comparative assessment of the flash-flood potential within small mountain catchments using bivariate statistics and their novel hybrid integration with machine learning models. *Science of the Total Environment* 711: 134514. DOI: https://doi.org/10.1016/j.scitotenv.2019.134514.

COSTACHE R and TIEN BUI D, 2019, Spatial prediction of flood potential using new ensembles of bivariate statistics and artificial intelligence: A case study at the Putna river catchment of Romania. *Science of the Total Environment* 691: 1098–1118. DOI: https://doi.org/10.1016/j.scitotenv.2019.07.197.

COSTACHE R and ZAHARIA L, 2017, Flash-flood potential assessment and mapping by integrating the weights-of-evidence and frequency ratio statistical methods in GIS environment – Case study: Bâsca chiojdului river catchment (Romania). *Journal of Earth System Science* 126(4): 59. DOI: https://doi.org/10.1007/s12040-017-0828-9.

CRUDEN DM and VARNES DJ, 1993, *Landslide Types and Processes*. U.S. National Academy of Sciences.

DASANTO BD, PRAMUDYA B, BOER R and SUHARNOTO Y, 2014, Effects of forest cover change on flood characteristics in the upper citarum watershed. *Jurnal Manajemen Hutan Tropika* 20(3): 141–149. DOI: https://doi.org/10.7226/jtfm.20.3.141.

Department of Food Crops and Horticulture West Java, 2024, Soil Type Delineation of West Java Province at a 1:250,000 Scale. In: Satu Peta Jabar. Available at: https://satupeta.jabarprov.go.id/maps?search=tanahandopenCatalog=true.

Department of Public Works and Spatial Planning Cianjur, 2022, Land Use/Land Cover Map of Cianjur Regency. Cianjur Regency Government.

DIAKAKIS M, BOUFIDIS N, SALANOVA GRAU JM, ANDREADAKIS E and STAMOS I, 2020, A systematic assessment of the effects of extreme flash floods on transportation infrastructure and circulation: The example of the 2017 Mandra flood. *International Journal of Disaster Risk Reduction* 47: 101542. DOI: https://doi.org/10.1016/j.ijdrr.2020.101542.

DUTAL H, 2023, Using morphometric analysis for assessment of flash flood susceptibility in the Mediterranean region of Turkey. *Environmental Monitoring and Assessment* 195(5): 582. DOI: https://doi.org/10.1007/s10661-023-11201-0.

ELSADEK WM and ALMALIKI AH, 2024, Integrated hydrological study for flash flood assessment using morphometric analysis and MCDA based on hydrological indices—Al-Sail Al-Kabir, KSA. *Natural Hazards* 120(7): 6853–6880. DOI: https://doi.org/10.1007/s11069-024-06450-2.

FAO, 2015, World reference base for soil resources 2014 International soil classification system for naming soils and creating legends for soil maps. In: Springer Water (3rd ed.). *Food and Agriculture Organization of the United Nations*. DOI: https://doi.org/10.1007/978-3-319-24409-9_25.

HANG HT, HOA PD, TRU VN and PHUONG NV, 2021, Application of Shannon'S Entropy Model and Gis in Flash Flood Forecasting Along National Highway-6, Hoa Binh Province, Vietnam. *International Journal of Geomate* 21(87): 50–57. DOI: https://doi.org/10.21660/2021.87.j2316.

HONG H, TSANGARATOS P, ILIA I, LIU J, ZHU AX and CHEN W, 2018, Application of fuzzy weight of evidence

and data mining techniques in construction of flood susceptibility map of Poyang County, China. *Science of the Total Environment* 625: 575–588. DOI: https://doi.org/10.1016/j.scitotenv.2017.12.256.

HORTON RE, 1945, Erosional development of streams and their drainage basins, hydrophysical approach to quantitative morphology. *Bulletin of The Geological Society of America* 56(3): 275–370. DOI: https://doi.org/10.1130/0016-7606(1945)56.

ISLAM S, TAHIR M and PARVEEN S, 2022, GIS-based flood susceptibility mapping of the lower Bagmati basin in Bihar, using Shannon's entropy model. *Modeling Earth Systems and Environment* 8(3): 3005–3019. DOI: https://doi.org/10.1007/s40808-021-01283-5.

JAIN SK, BEEVERS L, ANANDHI A and KUMAR DN, 2022, Multi-Disciplinary Approaches for Data Observation, Analysis, Forecasting, and Management. *Frontiers in Environmental Science* 10: 888906. DOI: https://doi.org/10.3389/fenvs.2022.888906.

JAVED A, KHANDAY MY and RAIS S, 2011, Watershed prioritization using morphometric and land use/land cover parameters: A remote sensing and GIS based approach. *Journal of the Geological Society of India* 78(1): 63–75. DOI: https://doi.org/10.1007/s12594-011-0068-6.

JEBUR MN, PRADHAN B and TEHRANY MS, 2014, Optimization of landslide conditioning factors using very high-resolution airborne laser scanning (LiDAR) data at catchment scale. *Remote Sensing of Environment* 152: 150–165. DOI: https://doi.org/10.1016/j.rse.2014.05.013.

JEHANZAIB M, AJMAL M, ACHITE M and KIM TW, 2022, Comprehensive Review: Advancements in Rainfall-Runoff Modelling for Flood Mitigation. *Climate* 10(10): 1–17. DOI: https://doi.org/10.3390/cli10100147.

KHOSRAVI K, POURGHASEMI HR, CHAPI K and BAHRI M, 2016, Flash flood susceptibility analysis and its mapping using different bivariate models in Iran: a comparison between Shannon's entropy, statistical index, and weighting factor models. *Environmental Monitoring and Assessment* 188(12): 656. DOI: https://doi.org/10.1007/s10661-016-5665-9.

KIA MB, PIRASTEH S, PRADHAN B, MAHMUD AR, SULAIMAN WNA and MORADI A, 2012, An artificial neural network model for flood simulation using GIS: Johor River Basin, Malaysia. *Environmental Earth Sciences* 67(1): 251–264. DOI: https://doi.org/10.1007/s12665-011-1504-z.

KURNIADI A, WELLER E, SALMOND J and ALDRIAN E, 2024, Future projections of extreme rainfall events in Indonesia. *International Journal of Climatology* 44(1): 160–182. DOI: https://doi.org/10.1002/joc.8321.

LI L, LAN H, GUO C, ZHANG Y, LI Q and WU Y, 2017, A modified frequency ratio method for landslide susceptibility assessment. *Landslides* 14(2): 727–741. DOI: https://doi.org/10.1007/s10346-016-0771-x.

LUBIS SW and RESPATI MR, 2021, Impacts of convectively coupled equatorial waves on rainfall extremes in Java, Indonesia. *International Journal of Climatology* 41(4): 2418–2440. DOI: https://doi.org/10.1002/joc.6967.

LUU C, HA H, BUI QD, LUONG ND, KHUC DT, VU H and NGUYEN DQ, 2023, Flash flood and landslide susceptibility analysis for a mountainous roadway in Vietnam using spatial modeling. *Quaternary Science Advances* 11: 100083. DOI: https://doi.org/10.1016/j.qsa.2023.100083.

MAHMOOD S and RAHMAN AU, 2019, Flash flood susceptibility modelling using geomorphometric approach in the Ushairy Basin, eastern Hindu Kush. *Journal of Earth System Science* 128(4): 1–14. DOI: https://doi.org/10.1007/s12040-019-1111-z.

MANSOUR A, MRAD D and DJEBBAR Y, 2024, Advanced modeling for flash flood susceptibility mapping using remote sensing and GIS techniques: a case study in Northeast Algeria. *Environmental Earth Sciences* 83(2): 1–19. DOI: https://doi.org/10.1007/s12665-023-11324-0.

MELTON MA, 1965, The Geomorphic and Paleoclimatic Significance of Alluvial Deposits in Southern Arizona. *The Journal of Geology* 73(1): 1–38.

MILLER VC, 1953, A Quantitative Geomorphic Study of Drainage Basin Characteristics in the Clinch Mountain Area, Virginia and Tennessee. Columbia University. *Department of Geology* Tech. Rept. 3(19). DOI: https://doi.org/10.1086/626413.

National Agency for Disaster Countermeasure, 2023, LAPORAN HARIAN: Selasa, 21 Maret.

OGAREKPE NM, NNAJI CC and EKPENYONG MG, 2022, Flash Flood Risk Assessment of the Great Kwa River Basin Using Analytical Hierarchy Process. *Water Conservation Science and Engineering* 7(4): 599–611. DOI: https://doi.org/10.1007/s41101-022-00167-8.

PRADHAN B, 2009, Groundwater potential zonation for basaltic watersheds using satellite remote sensing data and GIS techniques. *Central European Journal of Geosciences* 1(1): 120–129. DOI: https://doi.org/10.2478/v10085-009-0008-5.

RAHMAN MT, ALDOSARY AS, NAHIDUZZAMAN KM and REZA I, 2016, Vulnerability of flash flooding in Riyadh, Saudi Arabia. *Natural Hazards* 84(3): 1807–1830. DOI: https://doi.org/10.1007/s11069-016-2521-8.

RAHMATI O, POURGHASEMI HR and ZEINIVAND H, 2016, Flood susceptibility mapping using frequency

ratio and weights-of-evidence models in the Golastan Province, Iran. *Geocarto International* 31(1): 42–70. DOI: https://doi.org/10.1080/10106049.2015.1041559.

RAHMATI O, ZEINIVAND H and BESHARAT M, 2016, Flood hazard zoning in Yasooj region, Iran, using GIS and multi-criteria decision analysis. Geomatics, *Natural Hazards and Risk* 7(3): 1000–1017. DOI: https://doi.org/10.1080/19475705.2015.1045043.

SAMANTA RK, BHUNIA GS, SHIT PK and POURGHASEMI HR, 2018, Flood susceptibility mapping using geospatial frequency ratio technique: a case study of Subarnarekha River Basin, India. *Modeling Earth Systems and Environment* 4(1): 395–408. DOI: https://doi.org/10.1007/s40808-018-0427-z.

SARKAR D and MONDAL P, 2020, Flood vulnerability mapping using frequency ratio (FR) model: a case study on Kulik river basin, Indo-Bangladesh Barind region. *Applied Water Science* 10(1): 1–13. DOI: https://doi.org/10.1007/s13201-019-1102-x.

SAYAMA T, YAMADA M, SUGAWARA Y and YAMAZAKI D, 2020, Ensemble flash flood predictions using a high-resolution nationwide distributed rainfall-runoff model: case study of the heavy rain event of July 2018 and Typhoon Hagibis in 2019. *Progress in Earth and Planetary Science* 7(1): 75. DOI: https://doi.org/10.1186/s40645-020-00391-7.

SCHOENEBERGER P, WYSOCKI D, BUSSKOHL C and LIBOHOVA Z, 2017, Landscapes, Geomorphology, and Site Description. In: The Soil Survey Manual. *USDA Agriculture Handbook* 18: 21–82.

SCHUMM SA, 1956, Evolution of Drainage Systems and Slopes in Badlands at Perth Amboy, New Jersey. *Bulletin of the Geological Society of America* 67(5): 597–646. DOI: https://doi.org/10.1130/0016-7606(1956)67.

STRAHLER A, 1957, Quantitative Analysis of Watershed Geomorphology, Transactions of the American Geophysical Union. *Transactions, American Geophysical Union* 38(6): 913–920.

SUDJATMIKO, 2003, Geological Map of The Cianjur Quadrangle, Jawa Scale 1:100.000. Ministry of Energy and Mineral Resources.

TABARI H, 2020, Climate change impact on flood and extreme precipitation increases with water availability. *Scientific Reports* 10(1): 13768. DOI: https://doi.org/10.1038/s41598-020-70816-2.

TAHERIZADEH M, NIKNAM A, NGUYEN-HUY T, MEZŐSI G and SARLI R, 2023, Flash flood-risk areas zoning using integration of decision-making trial and evaluation laboratory, GIS-based analytic network process and satellite-derived information. *Natural Hazards* 118(3): 2309–2335. DOI: https://doi.org/10.1007/s11069-023-06089-5.

TEHRANY SM, PRADHAN B and JEBUR MN, 2013, Spatial prediction of flood susceptible areas using rule based decision tree (DT) and a novel ensemble bivariate and multivariate statistical models in GIS. *Journal of Hydrology* 504: 69–79. DOI: https://doi.org/10.1016/j.jhydrol.2013.09.034.

TEHRANY SM, KUMAR L, NEAMAH JEBUR M and SHABANI F, 2019, Evaluating the application of the statistical index method in flood susceptibility mapping and its comparison with frequency ratio and logistic regression methods. *Geomatics, Natural Hazards and Risk* 10(1): 79–101. DOI: https://doi.org/10.1080/19475705.2018.1506509.

UNISDR, 2015, The Human Cost of Weather Related Disasters 1995–2015. UNISDR.

VAN WESTEN CJ, 1997, *Statistical landslide hazard analysis. ILWIS 2.1 for Windows application guide*. ITC Publication.

WANG X, GOURBESVILLE P and LIU C, 2023, Flash Floods: Forecasting, Monitoring and Mitigation Strategies. *Water (Switzerland)* 15(9): 1–5. DOI: https://doi.org/10.3390/w15091700.

WANG X and LIU L, 2023, The Impacts of Climate Change on the Hydrological Cycle and Water Resource Management. *Water* 15(13): 2342. DOI: https://doi.org/10.3390/w15132342.

YALCIN A, 2008, GIS-based landslide susceptibility mapping using analytical hierarchy process and bivariate statistics in Ardesen (Turkey): Comparisons of results and confirmations. *Catena* 72(1): 1–12. DOI: https://doi.org/10.1016/j.catena.2007.01.003.

YULIANTO F, SUWARSONO NUGROHO UC, NUGROHO NP, SUNARMODO W and KHOMARUDIN MR, 2020, Spatial-Temporal Dynamics Land Use/Land Cover Change and Flood Hazard Mapping in the Upstream Citarum Watershed, West Java, Indonesia. *Quaestiones Geographicae* 39(1): 125–146. DOI: https://doi.org/10.2478/quageo-2020-0010.

Received 24 October 2024
Accepted 30 December 2024